MATERIALE PLASTICE
https://revmaterialeplastice.ro
https://doi.org/10.37358/Mat.Plast.1964

Polyethylene Terephthalate Nanofiber Mats for Barrier Membranes in Guided Bone Regeneration

MINGZHOU WU[#], JINJIE CHU[#], LI JIANG, ZHAOJUN WANG, TINGTING XU, FANGDONG SU, WENCHAO ZHOU, HUANHUAN FENG, LEI GU[*], PEIZHI HU[*]
Department of Orthopedics, Taicang TCM Hospital Affiliated to Nanjing University of Chinese Medicine, Taicang, 215400, China

Abstract: *Background: Barrier membranes prevent soft tissue invasion while promoting bone healing, suggesting a potential significance in guided bone regeneration (GBR). However, many resorbable membranes lack adequate mechanical strength and long-term stability. Polyethylene terephthalate (PET), a biostable polymer, exhibits promising properties for GBR but remains underexplored. Methods: Electrospun PET nanofiber membranes (PET-1 to PET-4) were fabricated by systematically varying solution concentrations and processing conditions. Their morphology was analyzed by scanning electron microscopy (SEM), and mechanical properties were assessed via tensile testing. Surface wettability was reflected by the water contact angle. In vitro biocompatibility was evaluated using the CCK-8 assay using L929 mouse fibroblasts. Barrier function was tested by Transwell and time-course fibroblast migration assays. Results: All PET membranes exhibited uniform nanofiber structures with good mechanical integrity. PET-4 showed the highest tensile strength (13.5 MPa) and elastic modulus (190 MPa). Contact angles ranged from 85° to 93°, which indicated moderate hydrophobicity. Cytocompatibility was high across all the groups, with PET-4 representing nearly 100% cell viability. In migration assays, PET-4 significantly suppressed fibroblast invasion over 48 h. Conclusion: Electrospun PET nanofiber membranes demonstrated excellent mechanical performance, cytocompatibility, and barrier function. PET-4 emerged as a particularly promising candidate for GBR application, offering effective long-term soft tissue exclusion and bone regeneration support.*

Keywords: *Electrospinning, fibroblast migration, nanofiber scaffold*

1. Introduction

Guided bone regeneration (GBR) is a widely adopted clinical technique to facilitate bone healing in periodontal defects, implant sites, and craniofacial reconstruction [1,2]. A critical component of GBR is the use of a barrier membrane that physically separates the bone defect area from surrounding soft tissues, thereby preventing fibroblast infiltration and maintaining a secluded space for osteogenic cell activity [3–5]. An ideal GBR membrane should satisfy multiple essential criteria, including adequate mechanical strength, long-term stability, biocompatibility, and selective permeability that blocks soft tissue invasion while allowing nutrient exchange to support bone regeneration [6,7].

Although resorbable membranes such as collagen and polylactic acid derivatives are commonly used in clinical practice, they still have significant limitations such as premature degradation, insufficient mechanical support, and unreliable barrier function [8,9]. Non-resorbable membranes provide enhanced mechanical durability and dimensional stability, but their clinical application requires careful optimization to ensure safety and functional integration [10–12]. Polyethylene terephthalate (PET) is an FDA-approved polymer that has been widely applied in biomedical implants such as vascular grafts, surgical meshes, and soft tissue patches due to its mechanical durability and long-term biostability [13–15]. In bone tissue engineering, PET has been utilized in periosteal expansion osteogenesis

*email: tczyy1210@163.com; hurenxizhen@126.com
[#]These authors contributed equally to this work

(PEO). Study showed that dense PET membranes coated with hydroxyapatite/gelatin and screw-fixed beneath the periosteum in rabbit mandibles has high biocompatibility and promotes new bone formation [16]. Furthermore, surface-modified PET materials incorporating chondroitin sulfate and polydopamine have been used as artificial grafts in ligament reconstruction. These modifications can regulate macrophage polarization, enhance stem cell recruitment, and promote osteogenic differentiation and immune microenvironment remodeling, ultimately facilitating graft-bone osseointegration [17]. While these findings confirmed the potential of PET in orthopedic applications, previous studies primarily focused on bulk PET structures or chemically modified surfaces used in non-barrier roles such as structural scaffolds or implant coatings. Crucially, these configurations lack nanofibrous architecture and adjustable porosity characteristics for functioning as a selective barrier membrane in GBR. It has been acknowledged that an ideal GBR membrane satisfy multiple criteria, including adequate mechanical strength, long-term dimensional stability, and selective cell exclusion while allowing nutrient and gas exchange to support osteogenesis [18]. Electrospinning can produce nanofibrous membranes that mimic extracellular matrix (ECM) and help maintain finely controlled mechanical and morphological characteristics [19,20]. Although PET has shown exceptional biostability, the development of electrospun PET nanofibers for GBR remains to be explored, and previous study only analyzed how electrospun PET membranes behave as physical barriers to resist fibroblast invasion, maintain long-term structure, and support biocompatibility.

In this study, we developed a series of electrospun PET nanofiber membranes (PET-1 to PET-4) with varying polymer concentrations, solvent systems, and processing conditions, and PET-4 was further treated by mild thermal annealing to enhance the fiber bonding. We systematically investigated their mechanical properties, surface wettability, cytocompatibility, and barrier function against fibroblast migration, aiming to identify a PET-based nanomembrane with optimal non-resorbable and long-lasting characteristics for GBR. This work distinguished itself from prior PET-based studies by introducing a scalable, structurally optimized electrospun configuration that provided both mechanical resilience and dynamic soft tissue exclusion in bone regeneration scenarios.

2. Materials and methods

2.1. Materials

Polyethylene terephthalate (PET, intrinsic viscosity 0.64 dL/g) was obtained from Sigma-Aldrich (Darmstadt, Germany). Hexafluoroisopropanol (HFIP), N,N-dimethylformamide (DMF), and other solvents were purchased from Aladdin (Shanghai, China). L929 mouse fibroblast cells and culture reagents including DMEM, FBS, and antibiotics were obtained from Gibco (Grand Island, America).

2.2. Preparation of PET nanofiber membranes

Four types of PET nanofiber membranes (PET-1 to PET-4) were prepared by electrospinning with different formulations and processing parameters. PET solutions (10–20 wt%) were dissolved in HFIP or HFIP/DMF (v/v = 9:1) under stirring at room temperature for 12 h. The electrospinning process was conducted using a 5 mL syringe equipped with a 21 G needle at 15–20 kV and a flow rate of 0.8–1.2 mL/h. The fibers were collected by a rotating drum collector (200–500 rpm) positioned 15–20 cm from the needle tip. Membrane thickness was strictly controlled by adjusting the collection duration (1–4 h). For PET-4, a mild thermal post-treatment (50°C, 2 h) was applied to enhance fiber bonding.

2.3. Scanning electron microscopy (SEM)

Membranes were sputter-coated with a gold layer and imaged using a field-emission scanning electron microscope (FESEM, Hitachi SU8010). Fiber diameter and morphology of at least 100 fibers per group were analyzed using ImageJ.

2.4. Mechanical testing

Tensile strength and elastic modulus were measured using a universal testing machine (Instron 5943). Membranes were cut into rectangular strips (10 mm × 30 mm) and tested at a strain rate of 5 mm/min. At least five replicates per group were measured.

2.5. Water contact angle measurement

Surface hydrophobicity was assessed using a contact angle goniometer (Krüss DSA25). Water droplet (3 µL) was placed on the membrane surface, and the static contact angle was recorded within 5 s of droplet stabilization. Each membrane was tested at three different locations.

2.6. Cytocompatibility assay

L929 cells were seeded at 1×10^4 cells/well into 96-well plates containing sterilized PET membranes. After 24-h incubation, cell viability was measured using CCK-8 assay (Dojindo) according to the manufacturer's instructions. Absorbance was read at 450 nm using a microplate reader (BioTek). The results were normalized to the control group (cells without membranes).

2.7. Transwell migration assay

To evaluate the barrier function, Transwell inserts (pore size: 8 µm, Corning) were coated with PET membranes. L929 fibroblasts (5×10^4 cells in 200 µL serum-free DMEM) were seeded into the upper chamber, whereas 600 µL of 10% FBS-containing medium was added to the lower chamber. After 24-h incubation, cells that migrated to the lower chamber were fixed, stained with crystal violet, and counted under a microscope.

2.8. Time-dependent cell invasion assay

To assess the dynamic barrier performance, similar Transwell setups were used. Briefly, the cells were fixed and stained at 6, 12, 24, and 48 h. Migration was quantified by counting invaded cells or by absorbance following dye extraction. All experimental values were normalized against the 6-h measurements obtained from control groups.

3. Results

As illustrated in Figure 1, a schematic diagram was designed to conceptually demonstrate the fabrication process and the intended application of the electrospun PET nanofiber membrane in a GBR setting. The left panel depicted the electrospinning process, wherein PET polymer solution was ejected under high voltage to form a nanofibrous membrane with a porous architecture. The right panel showed the application of the membrane to a bone defect where it served as a physical barrier to separate soft tissue from the defect area and created a protected space to facilitate osteogenic cell migration and bone regeneration. This figure summarized the design logic and translational potential of the PET membrane system in GBR applications. It should be noted that this figure was a conceptual illustration rather than an image derived from *in vivo* experimentation.

As illustrated in Figure 2, both the tensile strength and elastic modulus of PET nanofiber membranes increased progressively from PET-1 to PET-4. The tensile strength ranged from 8.5 to 13.5 MPa, while the elastic modulus increased from 120 to 190 MPa. PET-4 exhibited the highest mechanical performance among all the tested variants.

As shown in Figure 3, all PET nanofiber membranes exhibited moderate hydrophobicity, with water contact angles ranging from approximately 85° to 93°. PET-3 demonstrated the highest contact angle (92.7°), while PET-1 showed the lowest contact angle (85.3°). The trend suggested the hydrophobicity was gradually enhanced with modified membrane compositions and structures from PET-1 to PET-3, followed by a slight reduction in PET-4.

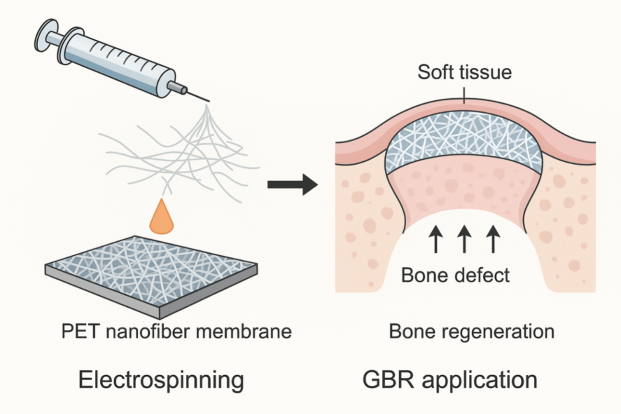

Figure 1. Schematic illustration of the fabrication of electrospun PET nanofiber membranes and their intended application as a barrier membrane in guided bone regeneration (GBR). This is a conceptual representation rather than an image derived from *in vivo* experimental data

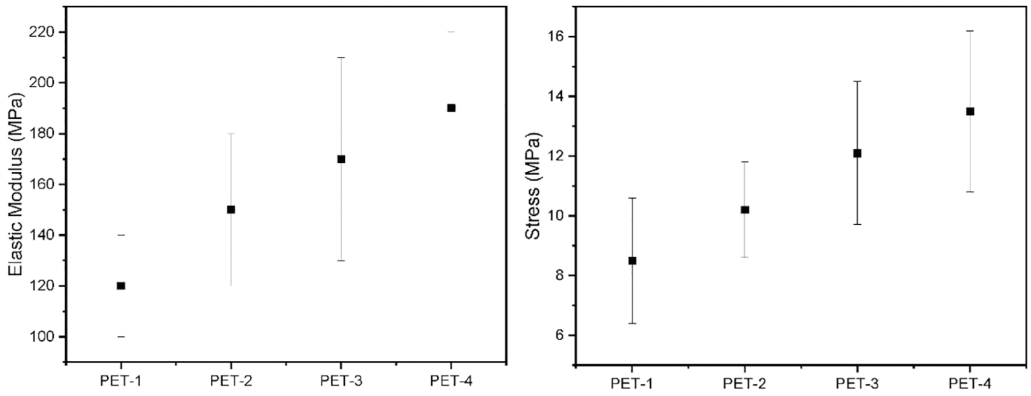

Figure 2. Mechanical properties of electrospun PET nanofiber membranes. The left panel showed the elastic modulus (MPa) and the right panel displayed the tensile strength (stress, MPa) of four different PET membranes (PET-1 to PET-4). Each data point represented the mean value with standard deviation (n = 5)

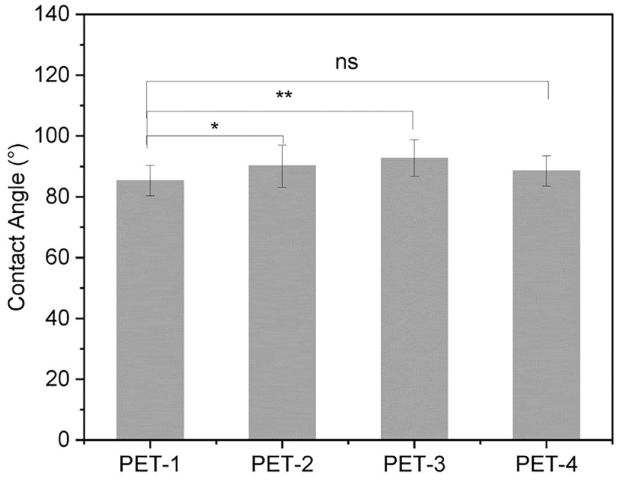

Figure 3. Water contact angle measurements of PET nanofiber membranes (PET-1 to PET-4), indicating differences in surface hydrophobicity (*$p < 0.05$, **$p < 0.01$, ns = not significant)

As shown in Figure 4, all PET membrane groups exhibited a relatively high cell viability, with values ranging from 0.92 to 1.00. A gradual increase in the cell viability from PET-1 to PET-4 was observed, with PET-4 showing a slightly higher cell viability than the controls. No significant cytotoxicity was detected in any of the membrane formulations.

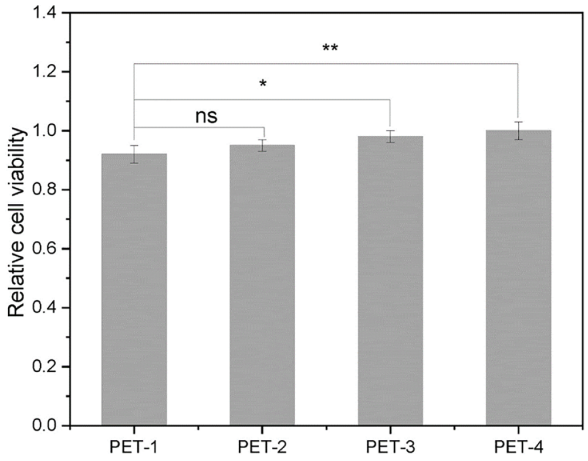

Figure 4. Relative cell viability of PET nanofiber membranes (PET-1 to PET-4) assessed by CCK-8 assay after 24-h incubation with L929 fibroblasts. All values were normalized to the control group (1.0) (*$p < 0.05$, **$p < 0.01$, ns = not significant)

As illustrated in Figure 5, the PET nanofiber membranes significantly reduced the migration of fibroblasts compared to the control group without membrane. PET-1 showed a relative migration value of approximately 0.35, while PET-4 demonstrated the strongest barrier effect as the migration was reduced to 0.18. A stepwise decrease in cell penetration from PET-1 to PET-4 was observed, indicating an improved barrier performance with optimized membrane properties.

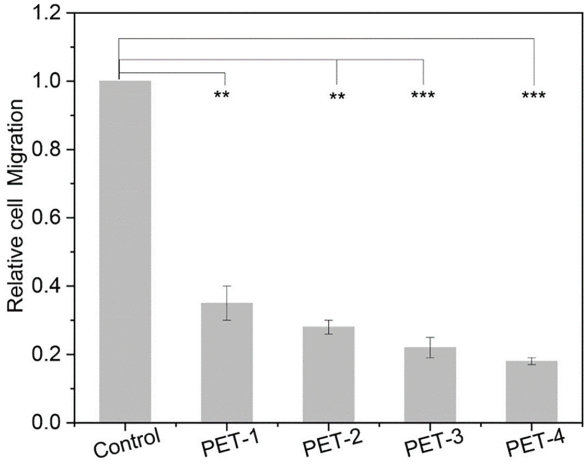

Figure 5. Relative cell migration across PET nanofiber membranes (PET-1 to PET-4) in Transwell assay using L929 mouse fibroblasts. The control group without membrane was set as 1.0 (**$p < 0.01$, ***$p < 0.001$)

Figure 6 showed that the migration of fibroblasts was steadily increased in all the groups over time, but the rate of migration was significantly suppressed in the PET membrane groups than the control. The control group showed a rapid rise in migration, exceeding over 4-fold by 48 h, whereas PET-1 to PET-4

demonstrated progressively enhanced invasion inhibition, culminating in maximal suppression efficacy in PET-4 (only ~1.3-fold increase at 48 h). All the PET groups exhibited a time-dependent yet moderate increases in cell migration, reflecting sustained but partial barrier activity.

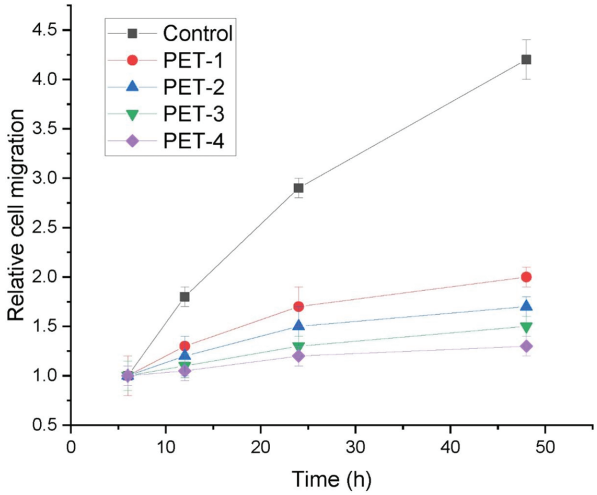

Figure 6. Time-dependent fibroblast invasion assay. Relative cell migration was quantified at 6, 12, 24, and 48 h across different PET membranes (PET-1 to PET-4) and a control group without membrane. Values were normalized to the baseline (6 h = 1.0)

As shown in Figure 7, the electrospun PET membrane exhibited a uniform network of randomly oriented, bead-free nanofibers with smooth surfaces. The average fiber diameter was within the submicron range (~200–400 nm), aligning with predetermined electrospinning parameters. Although direct measurement of pore size and porosity was not performed, the overall fiber arrangement suggested a highly interconnected and compact architecture. Notably, no visible defects or fused beads were observed throughout the field of view, indicating an adequate morphological integrity. The dense and well-organized fiber network may contribute to the barrier function by limiting inter-fiber spacing and restricting cell penetration. Future investigations incorporating atomic force microscopy (AFM) will be conducted to quantitatively assess surface topography and its relationship to wettability.

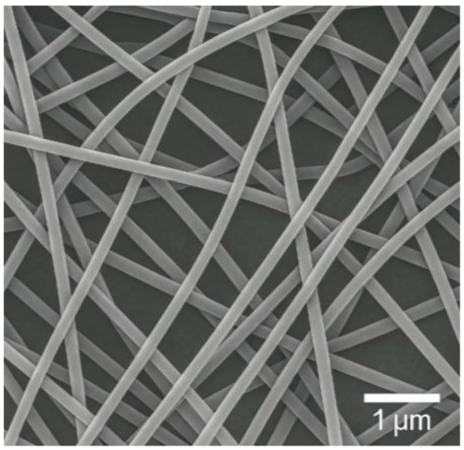

Figure 7. Representative scanning electron microscopy (SEM) image of electrospun PET nanofiber membrane. The fibers exhibited a smooth surface and randomly oriented network with uniform diameters. Scale bar = 1 µm

4. Discussion

The effectiveness of PET nanofiber membranes in GBR largely depends on their ability to serve as a selective barrier that physically prevents soft tissue infiltration while permitting osteogenic cell activity within the defect region. Electrospinning produces a nonwoven mat with high fiber density and small pore size, typically in the submicron to low micron range below the threshold required for fibroblast penetration. This structural feature is critical in maintaining a spatial boundary between the rapidly proliferating soft tissue and slowly forming bone tissue. In addition to the physical morphology, the intrinsic material properties of PET contribute significantly to its performance as a barrier membrane. The hydrophobicity of PET can reduce protein adsorption and cell adhesion of non-osteogenic lineages such as fibroblasts, thereby enhancing its anti-invasion capability. Moreover, PET exhibits high mechanical strength and dimensional stability, which allows the membrane to retain its form under physiological stresses and resist collapse into the defect space. This mechanical robustness creates and sustains a secluded space conducive to the key processes in bone regeneration, including osteoprogenitor recruitment, vascular infiltration, and extracellular matrix deposition. Furthermore, the biostability of PET offers advantages for clinical scenarios requiring sustained barrier functionality. Different from biodegradable membranes that may lose integrity at premature stage, PET maintains its structural and functional properties over extended durations and offers continuous protection for the regenerative site. Collectively, the nanofibrous architecture, mechanical resilience, hydrophobic surface, and slow degradation of the PET membranes all contribute to a reliable barrier functionality in GBR applications [21].

As is shown in Figure 2, the mechanical properties of electrospun PET membranes played a critical role in their function as barrier materials in GBR, and the observed differences among PET-1 to PET-4 reflected the influence of electrospinning parameters and formulation design [22,23]. Specifically, PET-1 was fabricated using a lower polymer concentration and shorter collection time, resulting in a looser fiber network with lower mechanical integrity [24]. In contrast, PET-4 was developed with higher polymer concentration (e.g., 18–20 wt%), optimized solvent system (e.g., HFIP/DMF mixture), and extended spinning duration, which collectively increased fiber density and yielded a more compact membrane architecture. Additionally, PET-4 underwent mild thermal annealing to induce partial fiber fusion at contact points, significantly enhancing inter-fiber bonding and mechanical stiffness. The gradual enhancement in both tensile strength and modulus across PET-1 to PET-4 was correlated with improved fiber alignment, reduced pore size, and increased thickness, which all contributed to a better load distribution under stress. Denser and more tightly packed networks are less prone to deformation or tearing, which is crucial for maintaining defect coverage and resisting physiological loading *in vivo*. From a functional perspective, the mechanical performance of PET-3 and PET-4 exceeded the minimum strength required for GBR membranes (e.g., >10 MPa tensile strength) while still preserving flexibility for surgical handling. Unlike collagen-based resorbable membranes, which tend to lose mechanical integrity rapidly after implantation, PET nanofiber membranes provide stable, long-term support due to their non-degradable nature and high modulus. Thus, by adjusting electrospinning formulation and processing conditions, the mechanical profile of PET membranes can be finely improved to balance flexibility and strength for specific clinical needs in guided tissue regeneration [25].

The surface hydrophobicity of PET nanofiber membranes is primarily influenced by fiber morphology, packing density, and surface roughness [26]. As the electrospinning parameters were optimized from PET-1 to PET-3, the resulting membranes in Figure 3 displayed more densely packed, uniform, and aligned fiber networks, which showed lower surface wettability and higher contact angle [26]. The enhanced hydrophobicity may help reduce early protein adsorption and nonspecific fibroblast attachment, thereby reinforcing the membrane's barrier function [27].

However, the slight reduction in the contact angle of PET-4 may result from increased membrane thickness or surface heterogeneity caused by thermal annealing, which can alter fiber surface chemistry or roughness. While all contact angles remained below the superhydrophobic threshold (>150°),

values above 90° suggested a favorable surface condition for minimizing soft tissue ingrowth while maintaining adequate permeability for nutrient diffusion. Together with mechanical stability, these surface characteristics can support the functional role of PET membranes in GBR.

The excellent cytocompatibility observed across all THE PET membranes confirmed that the base material and electrospinning process did not introduce cytotoxic effects. PET is an FDA-approved polymer widely used in biomedical implants, and its inert surface minimizes adverse cellular responses. The slight increase in the viability from PET-1 to PET-4 may result from smoother fiber morphology, reduced residual solvent content, or improved structural integrity during cell culture. Moreover, the nanofibrous structure provided a topography that supported cell attachment and spreading. The fact that PET-4 achieved nearly 100% viability indicated that optimized formulation and processing did not compromise cell safety. This biocompatibility is crucial for clinical GBR applications, given the direct contact of the membrane with periosteal and soft tissue layers [28]. These results further supported the promising potential of the PET to be used as a long-term implantable barrier material [29].

The ability of PET membranes to inhibit fibroblast migration is a key functional requirement for GBR, as soft tissue ingrowth into the defect site impedes bone formation [30]. The marked reduction in cell migration across all the PET groups confirmed the physical barrier capability of the nanofibrous architecture. A lower migration trend from PET-1 to PET-4 was correlated with improved membrane properties, including reduced pore size, higher fiber packing density, and increased mechanical stability [31]. These structural improvements are likely to hinder cell penetration by creating a denser and less permeable network while still allowing diffusion of nutrients and signaling molecules [32]. Notably, PET-4 with the highest barrier effect showed optimized fiber deposition and mild thermal crosslinking, which enhanced fiber cohesion and reduced inter-fiber gaps [33]. These findings validated that adjusting electrospinning parameters can effectively modulate the barrier function of PET membranes, which was the reason that allowed PET-4 to be considered as the most suitable candidate for bone regeneration applications requiring sustained exclusion of soft tissue [34].

Previous dynamic fibroblast invasion assay highlighted the temporal performance of PET nanofiber membranes in resisting cell penetration [35]. The pronounced distinction between the control and PET groups demonstrated that even at early time points, PET membranes can effectively slow down fibroblast infiltration. Among them, PET-4 consistently showed the slowest increase in relative migration, reflecting its superior physical barrier characteristics [36]. The reduced invasion in PET-4 can be attributed to its higher fiber density and uniform nanostructure, and potentially reduced pore interconnectivity, which all impeded cellular translocation through the membrane. The sustained suppression during 48-h period suggested that PET-4 could offer prolonged protection against soft tissue encroachment, a critical factor in successful GBR. These results indicated that adjusting electrospun membrane architecture can strategically optimized the time-dependent barrier function of PET membranes for regenerative applications [37].

The observed nanofibrous architecture is a critical feature involved in the functional performance of PET membranes in GBR. The submicron fiber size mimics native extracellular matrix (ECM), providing a favorable microenvironment for tissue integration. Dense fiber packing and randomly entangled structure create a physical barrier that can block cell infiltration while maintaining permeability for gas and nutrient exchange. The absence of defects or fused beads confirmed successful optimization of electrospinning parameters such as solution concentration, voltage, and collection distance. The uniformity in fiber diameter and morphology supported consistent mechanical performance and barrier function of the membrane. This structural profile is particularly important for long-term *in vivo* applications when sustained mechanical and morphological stability is required. Thus, the SEM findings validated the microstructural basis for the PET membrane's barrier, mechanical, and biocompatibility properties.

Also, some limitations existed in our research. First, in this study, the structural morphology information of the membrane was obtained by SEM observation, but the pore size, porosity and pore interconnectivity were not quantitatively analyzed. Therefore, the relationship between membrane

structure and its barrier performance (especially inhibition of fibroblast migration) remained to be explored. In subsequent studies, we will introduce advanced techniques such as micro-CT scanning or three-dimensional image reconstruction to quantitatively characterize the membrane structural parameters to establish a more rigorous "structure-function" correlation. In addition, we hypothesized in our discussion that reduced contact angle of PET-4 might be related to the change in surface topography after heat treatment, but the relevant inference lacked direct evidence as atomic force microscopy (AFM) or surface roughness testing was not performed in this study. In the future, we will analyze the nanostructural changes before and after heat treatment applying AFM and surface profilometry to further explore the mechanistic links between surface topography and biological behaviors such as wettability and protein adsorption. Finally, the present study was primarily based on *in vitro* evaluation. Although the barrier function was verified by cell migration experiments, the implantation effect, biointegration ability and bone regeneration promoted by the membrane during bone defect repair were not evaluated using animal model. Classical animal GBR model experiments will be carried out to systematically evaluate the membrane's biocompatibility, tissue integration and bone repair efficiency *in vivo*.

5. Conclusion

Electrospun PET nanofiber membranes demonstrated uniform structure, adequate mechanical strength, and excellent cytocompatibility. Among all variants, PET-4 showed the highest tensile properties, optimal hydrophobicity, and strongest barrier function against fibroblast migration. These findings indicated that PET nanofiber membranes, especially PET-4, were promising candidates for non-resorbable GBR applications due to their mechanical stability and effective soft tissue exclusion.

Acknowledgement: Not applicable.

Funding Statement: This research was funded by the Basic Research Project of Medical Innovative Application in Suzhou (SKYD2023071) and the Basic Research Program of Medical Application in Suzhou (SKYD2023238).

Author Contributions: The authors confirm contribution to the paper as follows: study conception and design: Lei Gu, Peizhi Hu; data collection: Mingzhou Wu, Jinjie Chu; analysis and interpretation of results: Li Jiang, Zhaojun Wang, Tingting Xu; draft manuscript preparation: Fangdong Su, Wenchao Zhou, Huanhuan Feng. All authors reviewed the results and approved the final version of the manuscript.

Availability of Data and Materials: The data that support the findings of this study are available from the Corresponding Authors, Lei Gu, Peizhi Hu, upon reasonable request

Ethics Approval: Not applicable.

Conflicts of Interest: The authors declare no conflicts of interest to report regarding the present study.

References

1. Astaneh ME, Noori F, Fereydouni N. Curcumin-loaded scaffolds in bone regeneration. Heliyon. 2024;10(11):e32566. doi:10.1016/j.heliyon.2024.e32566.
2. Bauso LV, La Fauci V, Longo C, Calabrese G. Bone tissue engineering and nanotechnology: a promising combination for bone regeneration. Biology. 2024;13(4):237. doi:10.3390/biology13040237.
3. Bektas C, Mao Y. Hydrogel microparticles for bone regeneration. Gels. 2024;10(1):28. doi:10.3390/gels10010028.
4. Beloti MM, Rosa AL. Bone regeneration and repair materials. J Funct Biomater. 2024;15(3):78. doi:10.3390/jfb15030078.

5. Guo Y. Mechanism of exendin-4 promoting bone regeneration. In: Third International Conference on Biological Engineering and Medical Science (ICBioMed2023). Bellingham, WD, USA: SPIE; 2024. 129240R.
6. Castro JI, Payan-Valero A, Valencia-Llano C-H, Zapata MEV, Hernandez JHM, Zapata PA, et al. Graphene oxide nanosheets for bone tissue regeneration. Molecules. 2024;29(14):3263. doi:10.3390/molecules29143263.
7. Duarte ND, Frigerio PB, Chica GEA, Okamoto R, Buchaim RL, Buchaim DV, et al. Biomaterials for guided tissue regeneration and guided bone regeneration: a review. Dent J. 2025;13(4):179. doi:10.3390/dj13040179.
8. Gulab H, Malik S, Hussain K. Catalytic pyrolysis of polyethylene terephthalate and its copyrolysis with polyethylene. Environ Eng Sci. 2024;41(8):327–36. doi:10.1089/ees.2024.0006.
9. Dross M, Ehleben M, Droeder K. Mineral filler hybridization in recycled polyethylene terephthalate. Polymers. 2025;17(3):259. doi:10.3390/polym17030259.
10. Li A, Li Z, Liang Y, He Y, Jiang X. Optimized piezoelectric bone regeneration through inhibiting sympathetic nerve-bone interaction. Surf Interfaces. 2024;48:104380. doi:10.1016/j.surfin.2024.104380.
11. Li J, An Z, Kong Y, Zhang L, Yang J, Wang X, et al. Selective recovery of para-xylene from polyethylene terephthalate plastic. Appl Catal B-Environ Energy. 2024;357:124307. doi:10.1016/j.apcatb.2024.124307.
12. Le Grill S, Brouillet F, Drouet C. Bone regeneration: mini-review and appealing perspectives. Bioengineering. 2025;12(1):38. doi:10.3390/bioengineering12010038.
13. Kawai F, Iizuka R, Kawabata T. Engineered polyethylene terephthalate hydrolases: perspectives and limits. Appl Microbiol Biotechnol. 2024;108(1):404. doi:10.1007/s00253-024-13222-2.
14. Guo Z, Zhang H, Chen H, Zhang M, Tang X, Wang M, et al. Hydrogenating polyethylene terephthalate into degradable polyesters. Angewandte Chemie-Int Edit. 2025;64(6):e202418157. doi:10.1002/ange.202418157.
15. Holliday LS, Neubert JK, Yang X. Gas-powered extracellular vesicles promote bone regeneration. Extracell Ves Circulat Nucl Acids. 2025;6(1):158–65. doi:10.20517/evcna.2024.91.
16. Imoto K, Hoshi K, Odashima K, Nogami S, Unuma H, Yamauchi K. Static and dynamic guided bone regeneration using a shape-memory polyethylene terephthalate membrane: an experimental study in rabbit mandible. Clini Imp Dent Relat Res. 2024;26(4):734–41. doi:10.1111/cid.13337.
17. Li YM, Wu JY, Jiang J, Dong SK, Chen YS, He HY, et al. Chondroitin sulfate-polydopamine modified polyethylene terephthalate with extracellular matrix-mimetic immunoregulatory functions for osseointegration. J Mat Chem B. 2019;7(48):7756–70. doi:10.1039/d0tb90152k.
18. Yang Z, Wu C, Shi H, Luo X, Sun H, Wang Q, et al. Advances in barrier membranes for guided bone regeneration techniques. Front Bioeng Biotechnol. 2022;10:921576. doi:10.3389/fbioe.2022.921576.
19. Li R, Xu S, Guo Y, Cao C, Xu J, Hao L, et al. Application of collagen in bone regeneration. J Orthop Translat. 2025;50(7):129–43. doi:10.1016/j.jot.2024.10.002.
20. Li S, Yang Y, Yu B, Gao X, Gao X, Nie S, et al. A novel deer antler-inspired bone graft triggers rapid bone regeneration. Adv Mater Weinheim. 2025;37(6):e2411571. doi:10.1002/adma.202411571.
21. Zhen C, Shi Y, Wang W, Zhou G, Li H, Lin G, et al. Advancements in gradient bone scaffolds: enhancing bone regeneration in the treatment of various bone disorders. Biofabrication. 2024;16(3). doi:10.1088/1758-5090/ad4595.
22. Li X-L, Zhao Y-Q, Miao L, An Y-X, Wu F, Han J-Y, et al. Strategies for promoting neurovascularization in bone regeneration. Mil Med Res. 2025;12(1):9.

23. Liu A, Yang G, Zhao Y, Deng J, Liu J, Zhang K, et al. Bone-targeted hybrid extracellular vesicles for alveolar bone regeneration. Interdiscip Med. 2025;3(3):e20240126. doi:10.1002/inmd.20240126.
24. Liu R, Wang G, Ma L, Yang G, Lin S, Sun N, et al. An axolotl limb regeneration-inspired strategy to enhance alveolar bone regeneration. Bioact Mater. 2025;48(3):242–56. doi:10.1016/j.bioactmat.2025.02.020.
25. Xu Z, Wang J, Gao L, Zhang W. Hydrogels in alveolar bone regeneration. ACS Biomat Sci Eng. 2024;10(12):7337–51. doi:10.1021/acsbiomaterials.4c01359.
26. Morais AMMB, Martins VF, Alves AJ, Pocas F, Morais RMSC. Packaging and storage of Porphyridium cruentum: metallised polyethylene terephthalate/polyethylene (PETmet/PE) versus polyethylene (PE). Acta Alimentaria. 2024;53(3):419–31. doi:10.1556/066.2024.00093.
27. Lyu W, Zhang Y, Ding S, Li X, Sun T, Luo J, et al. A bilayer hydrogel mimicking the periosteum-bone structure for innervated bone regeneration. J Mat Chem B. 2024;12(43):11187–201. doi:10.1039/d4tb01923g.
28. Shim G-J, Lee CO, Lee J-T, Jung H-M, Kwon T-G. Potentiating effect of AMD3100 on bone morphogenetic protein-2 induced bone regeneration. Maxillofac Plast Reconstr Surg. 2024;46(1):22. doi:10.1186/s40902-024-00431-y.
29. Shanbhag S, Sanz-Esporrin J, Kampleitner C, Lie S-A, Gruber R, Mustafa K, et al. Peri-implant bone regeneration in pigs. Int J Implant Dent. 2024;10(1):55. doi:10.1186/s40729-024-00572-9.
30. Song P, Zhou D, Wang F, Li G, Bai L, Su J. Programmable biomaterials for bone regeneration. Mater Today Bio. 2024;29:101296. doi:10.1016/j.mtbio.2024.101296.
31. Souto-Lopes M, Grenho L, Manrique Y, Dias MM, Lopes JCB, Fernandes MH, et al. Bone regeneration driven by a nano-hydroxyapatite/chitosan composite bioaerogel for periodontal regeneration. Front Bioeng Biotechnol. 2024;12:1355950. doi:10.3389/fbioe.2024.1355950.
32. Steltzer SS, Abraham AC, Killian ML. Interfacial tissue regeneration with bone. Curr Osteopor Rep. 2024;22(2):290–8. doi:10.1007/s11914-024-00859-1.
33. Tang X, Zhou F, Wang S, Wang G, Bai L, Su J. Bioinspired injectable hydrogels for bone regeneration. J Adv Res. 2024;394(10206):1365. doi:10.1016/j.jare.2024.10.032.
34. Villicana C, Su N, Yang A, Tong X, Lee HP, Ayushman M, et al. Incorporating bone-derived ECM into macroporous microribbon scaffolds accelerates bone regeneration. Adv Healthc Mater. 2025;14(6):2402138. doi:10.1002/adhm.202402138.
35. Wang J, Cui Y, Zhang B, Sun S, Xu H, Yao M, et al. Polydopamine-Modified functional materials promote bone regeneration. Mater Design. 2024;238:112655. doi:10.1016/j.matdes.2024.112655.
36. Wang L-H, Lan S, Huang Z-B, Yang J-Y, Gong J-H, Yuan P-Q. Reaction kinetic model of glycolysis of polyethylene terephthalate. Chem Eng Sci. 2025;309(1):121463. doi:10.1016/j.ces.2025.121463.
37. Wang Y, Chen C, Zhang C, Cheng J, An B, Zhang N, et al. 3D bioprinting for tendon-bone interface regeneration. Int J Bioprint. 2025;11(2):164–83. doi:10.36922/ijb.8411.

Received: 28 May 2025; Accepted: 05 August 2025; Published: 30 September 2025